PI3K-C2β limits mTORC1 signaling and angiogenic growth

Piotr Kobialka[1,†], Judith Llena[1,†], Nerea Deleyto-Seldas[2], Margalida Munar[1], Jose A. Dengra[1], Pilar Villacampa[1], Alba Albinyà[1], Laia Muixi[1], Jorge Andrade[3,4], Hielke van Splunder[1], Ana Angulo-Urarte[1], Michael Potente[3,4], Joaquim Grego-Bessa[1], Sandra D. Castillo[1], Bart Vanhaesebroeck[5], Alejo Efeyan[2], Mariona Graupera[1,6,7,*]

[1]Endothelial Pathobiology and Microenvironment Group, Josep Carreras Leukaemia Research Institute (IJC), 08916 Badalona, Barcelona, Catalonia, Spain
[2]Metabolism and Cell Signaling Laboratory, Spanish National Cancer Research Centre (CNIO), Melchor Fernandez Almagro 3, Madrid 28029, Spain.
[3]Angiogenesis & Metabolism Laboratory, Berlin Institute of Health at Charité – Universitätsmedizin Berlin, 10178 Berlin, Germany.
[4]Max Delbrück Center for Molecular Medicine in the Helmholtz Association, 13125 Berlin, Germany.
[5]Cancer Institute, Paul O'Gorman Building, University College London, WC1N 1EH London, United Kingdom
[6]ICREA, Institució Catalana de Recerca i Estudis Avançats, Pg. Lluís Companys 23, 08010 Barcelona, Spain
[7]CIBERONC, Instituto de Salud Carlos III, Av. de Monforte de Lemos, 5, 28029 Madrid, Spain

[†] Equal contribution

[*]To whom correspondence should be addressed: M.G.
(mgraupera@carrerasresearch.org) Tel: +34 93 557 2800 Ext 4440

Abstract

Phosphoinositide 3-kinases (PI3Ks) phosphorylate intracellular inositol lipids to regulate signaling and intracellular vesicular trafficking. Mammals have eight PI3K isoforms, of which class I PI3Kα and class II PI3K-C2α are essential for vascular development. The class II PI3K-C2β is also abundant in endothelial cells. Here, using in vivo and in vitro approaches, we found that PI3K-C2β was a critical regulator of blood vessel growth by restricting endothelial mTORC1 signaling. Mice expressing a kinase-dead form of PI3K-C2β displayed enlarged blood vessels without corresponding changes in endothelial cell proliferation or migration. Instead, inactivation of PI3K-C2β resulted in an increase in the size of endothelial cells, particularly in the sprouting zone of angiogenesis. Mechanistically, we showed that the aberrantly large size of PI3K-C2β mutant endothelial cells was caused by mTORC1 activation, which sustained growth in these cells. Consistently, pharmacological inhibition of mTORC1 with rapamycin normalized vascular morphogenesis in PI3K-C2β mutant mice. Together, these results identify PI3K-C2β as a crucial determinant of endothelial signaling and illustrate the importance of mTORC1 regulation during angiogenic growth.

Introduction

Tissue morphogenesis and growth are sustained by the expansion of a hierarchically branched network of blood vessels that ensure efficient delivery of oxygen and nutrients (*1-3*). Endothelial cells line the inner wall of blood vessels, which expand through a process known as angiogenesis. When angiogenesis is altered, it contributes to multiple pathological conditions such as ischemic and inflammatory disorders, cancer, and overgrowth syndromes (*1-5*). Angiogenesis largely occurs through the formation of vascular sprouts followed by their anastomosis and remodeling (*6*). Later, redundant vessels are removed by a process called vascular pruning that ultimately allows the establishment of the hierarchical vascular tree (*6, 7*). The formation, expansion and remodeling of de novo sprouts require tight coordination between cell migration, growth, proliferation, matrix adhesion and cell-cell signaling processes (*6, 7*). The mechanism through which endothelial cells control their size and shape during these processes to maintain structural and functional integrity remains poorly understood.

Phosphoinositide 3-kinases (PI3Ks) are lipid kinases that generate a pool of phosphatidylinositol derivatives, all phosphorylated at the third position of the inositol headgroup (*8, 9*). The PI3K family comprises eight isoforms grouped into three classes based on their substrate preferences and structure (*8, 10*). The class I PI3Ks are activated by extracellular signals and produce phosphatidylinositol(3,4,5)trisphosphate (PIP_3) at the plasma membrane (*8, 9*). Through this lipid, class I PI3Ks activate many cellular functions, including cell proliferation, growth, migration and survival. Class II PI3Ks (PI3K-C2α, PI3K-C2β, and PI3K-C2γ) regulate vesicular trafficking and membrane dynamics by producing phosphatidylinositol(3,4)biphosphate (PIP_2) and phosphatidylinositol(3)phosphate (PI3P) in different intracellular sub-compartments (*10, 11*). Specifically, PI3K-C2α operates at the plasma membrane where it participates in clathrin-dependent endocytosis and facilitates early endosomal sorting and recycling (*11-14*). PI3K-C2β regulates insulin receptor endosomal trafficking, the mammalian target of rapamycin complex 1 (mTORC1) activity in late endosomes, and cell adhesion disassembly at focal sites (*15-17*). The physiological context in which these phospholipid-driven cellular functions are at play is, however, less clear.

78 PI3Ks are pivotal regulators in the vasculature, which control different aspects
79 of angiogenesis in an isoform-specific manner (*5*). Among the four class I PI3Ks
80 isoforms (PI3Kα, β, δ, and γ), PI3Kα is the key isoform in the function of angiogenic
81 endothelial cells in development and disease (*4, 18, 19*). PI3K-C2α is also essential
82 for vascular development in a cell-autonomous manner through the regulation of VE-
83 cadherin trafficking and vascular integrity (*20*). PI3K-C2β signaling controls vascular
84 leakage and edema under pathological stress conditions such as ischemic stroke and
85 inflammatory responses (*21*). Although PI3K-C2β is abundantly expressed in
86 endothelial cells (*21, 22*), whether PI3K-C2β-induced signaling contributes to vascular
87 development and angiogenesis remains to be explored.
88 In the present study, we used knock-in mice expressing a kinase-dead mutant
89 form of the PI3K-C2β protein to study the role of this lipid kinase in physiological
90 vascular development. We showed that inactivation of PI3K-C2β resulted in
91 hyperactive mTORC1 and exacerbated endothelial cell growth, thereby resulting in
92 abnormally dense blood vessels. Mechanistically, we found that loss of PI3K-C2β
93 activity stimulated mTORC1 signaling when either growth factors or amino acids were
94 deprived. Our data uncover a PI3K-C2β/mTORC1 axis that controls endothelial cell
95 growth during vascular expansion.
96
97
98 **Results**
99 **PI3K-C2β inactivation results in enlarged blood vessels**.
100 To investigate whether PI3K-C2β contributes to angiogenesis, we used mice
101 that express a catalytically inactive form of PI3K-C2β as a result of the introduction of
102 a germline kinase-inactivating D1212A point mutation (hereafter called $C2\beta^{KI/KI}$ mice)
103 (Fig. 1A), a model that faithfully leads to full inactivation of PI3K-C2β at the organismal
104 level (*17, 21*). $C2\beta^{KI/KI}$ mice are viable and fertile, providing an ideal experimental
105 system to study the impact of inactivation of this enzyme in vivo (*17*).
106 We focused on retinal angiogenesis, a key model to study signaling during
107 vessel growth in mice (*19, 20, 23*). Within the first week of age after birth, the vascular
108 network gradually expands from the center of the retina towards its periphery in a "two-
109 dimensional" fashion, providing an established screening platform for angiogenic
110 phenotypes using genetic models (*24*). We started our investigations by monitoring

111 vessel growth and architecture in whole-mount retinas between postnatal day (P) 3
112 and 8 upon full inactivation of PI3KC2β. These studies revealed a progressive
113 increase in vascular diameter and vascular density in C2$\beta^{KI/KI}$ retinas (Fig. 1B). Indeed,
114 although the vasculature of C2$\beta^{KI/KI}$ P3 retinas resembled that of controls (Fig. 1B),
115 mutant P6 retinas exhibited vascular tubes with larger diameter (Fig. 1B,C and fig.
116 S1A), a phenotype not associated with perturbations in total vascular area at P6 (Fig.
117 1D). Two days later, C2$\beta^{KI/KI}$ vessels had become even wider, leading to a substantial
118 increase in overall vascular density (Fig. 1B-D and fig. S1A). This phenotype was
119 largely observed in veno-capillary areas (Fig. 1E,F and fig. S1B), which is consistent
120 with venous endothelial cells being more proliferative than arterial endothelial cells
121 during angiogenic growth (*25, 26*). Other parameters, such as radial expansion or the
122 number of sprouts, remained unchanged in C2$\beta^{KI/KI}$ retinas at all the timepoints
123 investigated (Fig. S1C,D). Together, these data suggest an important role for PI3K-
124 C2β in angiogenesis. Of note, the phenotype of C2$\beta^{KI/KI}$ retinas was resolved when
125 angiogenesis was completed (fig. S1E,F), thereby indicating that PI3K-C2β regulation
126 largely occurs during angiogenesis and to a lesser extent during homeostatic
127 conditions.
128 A PI3K-induced increase in vessel diameter has been previously associated
129 with an increased number of endothelial cells (*27, 28*). Hence, we next assessed
130 whether the progressive phenotype of P8 C2$\beta^{KI/KI}$ retinas was the result of an increase
131 in endothelial cell proliferation. We analyzed the number of endothelial cells in S-phase
132 by injecting EdU to P8 pups 2 h prior to retinal isolation. However, no overt differences
133 in the number of EdU-positive endothelial cells was observed between control and
134 C2$\beta^{KI/KI}$ littermate retinas (Fig. 1G,H). In line with this finding, the total number of
135 endothelial cells was unaltered between genotypes (Fig. 1I,J). Staining of retinas for
136 phospho-histone H3, a bona fide readout of cell-cycle progression during mitosis,
137 confirmed these findings (fig. S1G,H). We also ruled out that an increase in endothelial
138 cell proliferation at P6, prior to the appearance of the enhanced vascular area,
139 accounted for the phenotype in C2$\beta^{KI/KI}$ retinas (fig. S1I,J). Although proliferation is
140 essential for vascular expansion (*26*), other cellular mechanisms such as impaired
141 motility also contribute to vessel enlargement (*29, 30*). However, radial expansion (a
142 measure of collective cell migration during angiogenesis) was similar between control
143 and C2$\beta^{KI/KI}$ mice (fig. S1C), suggesting that vessel enlargement induced by PI3K-C2β

144 inactivation is not associated with defects in endothelial cell proliferation and migration
145 in vivo.
146
147 **PI3K-C2β signaling regulates endothelial cell growth**.
148 Tissue expansion requires tight coordination between cell growth and cell
149 division (*31-33*). In the absence of alterations in cell proliferation, we hypothesized that
150 the abnormal width of C2β$^{KI/KI}$ blood vessels is caused by the growth of individual
151 endothelial cells in part because PI3K-C2β knockdown in human embryonic kidney
152 293T cells results in accelerated cell growth (*15, 34*). To test our hypothesis, we used
153 human umbilical vein endothelial cells (HUVECs) in which PI3K-C2β was knocked
154 down by RNA interference (siRNA) (Fig. 2A,B) as well as mouse lung endothelial cell
155 (MLECs) isolated from control and C2β$^{KI/KI}$ mice. Both control and C2β$^{KI/KI}$ mouse
156 endothelial cells showed similar expression levels of PI3K-C2β (fig. S2A). Consistent
157 with the retinal data, neither PI3K-C2β depletion (in human cells) nor inactivation (in
158 mouse cells) affected endothelial cell proliferation in vitro (Fig. 2C,D and fig. S2B,C).
159 Collective endothelial cell migration was also unaffected (Fig. 2E,F and fig. S2D,E).
160 Instead, loss of PI3K-C2β protein or activity resulted in a significant increase in cell
161 size, both in confluent and sparse human and mouse endothelial cells (Fig. 2G-J and
162 fig. S2F-I). These data suggest that PI3K-C2β-deficient cells exhibit an intrinsic cell
163 growth phenotype rather than a cell spreading defect. In line with this notion, analysis
164 by flow cytometry confirmed that PI3K-C2β-null cells were larger (fig. S2J). To monitor
165 the effect of PI3K-C2β inactivation on endothelial cell growth during vascular
166 development, we crossed the C2β$^{KI/KI}$ mice with the ROSA^{mTmG};*Pdgfb*-iCreER mice
167 (hereafter called EC-mTmG) (*35, 36*). This genetic strategy allows the expression of
168 cell membrane-localized EGFP specifically in endothelial cells (Pdgfb-iCreER) upon
169 treatment with 4-hydroxytamoxifen (4-OHT) (Fig. 2K). To assess cell size in individual
170 cells, we labeled single cells by injecting P6 mice with a low dose of 4-OHT and
171 analyzed retinas at P8 (Fig. S2K) (*23*). Genetic in vivo inactivation of PI3K-C2β during
172 angiogenesis resulted in larger cells, as compared to wild-type endothelial cells (Fig.
173 2L,M). Collectively, these data are consistent with a cell growth-promoting effect in
174 endothelial cells with defective PI3K-C2β signaling. Given that both kinase-dead
175 (mouse) and expression knock-down (human) cells produced similar results, our data
176 suggest that this process is supported by the lipid kinase-related activity of PI3K-C2β.

177

178 **Inactivation of PI3K-C2β results in mTORC1 hyperactivation**.

179 To gain mechanistic insight into how PI3K-C2β inactivation leads to alterations
180 in cell growth, we performed intracellular signaling perturbations in control and PI3K-
181 C2β mutant endothelial cells. Inactivation of PI3K-C2β results in enhanced AKT and
182 mTORC1 signaling by two independent mechanisms (*15, 17*). Enhanced
183 phosphorylation of AKT upon inactivation of PI3K-C2β relates to an amplification of
184 insulin-induced class I PI3K-dependent AKT signaling (*17*). Instead, mTORC1
185 overactivation upon depletion of PI3K-C2β is a result of impaired mTORC1
186 downregulation, an effect that occurs in an AKT-independent manner (*15*). Because
187 mTORC1 is a master regulator of cell growth in most cells, (*32*) including endothelial
188 cells (*37, 38*), we postulated that inactivation of PI3K-C2β signaling in endothelial cells
189 leads to enhanced mTORC1 activity and thus to increased endothelial cell growth. We
190 assessed mTORC1 activity using antibodies that recognized Thr^{389}-phosphorylated
191 S6 kinase (S6K, a downstream target of mTORC1) and $Ser^{235/236}$-phosphorylated S6
192 (a substrate of S6K). PI3K-C2β-deficient HUVECs and PI3K-C2β kinase-dead MLECs
193 showed a substantial increase in the phosphorylation of S6K and S6 without changes
194 in that of AKT (Fig. 3A,B and fig. S3A,B). The phosphorylation of S6K and S6 was
195 blocked by the allosteric mTOR inhibitor rapamycin (Fig. 3C,D), confirming that the
196 activation of S6K and S6 depends on mTORC1. mTORC1-regulation of cell growth
197 requires the anchorage of mTORC1 to lysosomes where it orchestrates an anabolic
198 program (*32*). Under starvation conditions, PI3K-C2β is recruited to late endosomes
199 and lysosomes where it binds to the regulatory-associated protein of mTOR (Raptor).
200 This association represses mTORC1 activity by promoting the binding of Raptor with
201 inhibitory 14-3-3 proteins (*15*). Hence, we next wondered whether inactivation of PI3K-
202 C2β in endothelial cells interfered with mTOR localization. To address this, we
203 performed co-staining for mTOR and the lysosomal marker LAMP2 in endothelial cells
204 depleted of PI3K-C2β (Fig. 3E). As revealed by Pearson correlation analysis,
205 colocalization of mTORC1 and LAMP2 was similar in control and PI3K-C2β-deficient
206 HUVECs at steady state (Fig. 3F). Instead, we noticed that mTOR and LAMP2
207 colocalized in the peripheral regions of PI3K-C2β depleted HUVECs rather than close
208 to nuclei in control cells (Fig. 3E,G,H). These data align with observations that

209 peripheral localization of lysosomes is associated with increased mTORC1 signaling
210 (*39*).
211 As described in HeLa cells (*15*), high mTORC1 activity induced by loss of PI3K-
212 C2β is also observed under starvation conditions (fig. S3C-F). Given that mTORC1
213 regulates cell growth by integrating various environmental cues (*32, 40*), we next
214 explored the signals under which PI3K-C2β repressed mTORC1 activity in endothelial
215 cells. To this end, PI3K-C2β-depleted HUVECs were cultured in medium without
216 growth factors or amino acids, as previously described (*41*). We found that mTORC1
217 activity in the absence of PI3K-C2β was increased when either growth factors or amino
218 acids were depleted (Fig. 4A-D). As expected, prolonged amino acid deprivation led
219 to a shutdown of mTORC1 signaling (Fig. 4C,D). PI3K-C2β depletion also facilitated
220 the recovery of mTORC1 activity after starvation and replenishment of growth factors
221 or amino acids (Fig. 4E-H). The recovery was faster in PI3K-C2β deficient endothelial
222 cells, most likely because mTORC1 activity was higher in these cells under starvation
223 conditions (Fig. 4E-H). We also noticed that the differences between control and PI3K-
224 C2β deficient endothelial cells were greater upon replenishment of growth factor than
225 amino acids, suggesting that PI3K-C2β preferentially regulates mTORC1 downstream
226 of growth factors. In line with this notion, PI3K-C2β-depleted HUVECs showed a
227 greater increase in mTORC1 signaling upon stimulation with vascular endothelial
228 growth factor A (VEGF-A), the master regulator of angiogenesis, compared to control
229 cells (fig. S4, A and B).
230
231 **Rapamycin normalizes vascular morphogenesis in PI3K-C2β deficient mice.**
232 We next explored whether PI3K-C2β-related regulation of mTORC1 signaling
233 operates during angiogenesis. To address this question, we assessed the
234 phosphorylation of S6 in $C2\beta^{KI/KI}$ retinas and found that phosphorylation of $Ser^{235/236}$
235 and $Ser^{240/244}$ were substantially increased upon PI3K-C2β inactivation in growing
236 vessels (Fig. 5A,B and fig. S5A,B). We noticed that overactivation of mTORC1
237 signaling in $C2\beta^{KI/KI}$ retinas was most prominent at the sprouting front compared to the
238 remodeling area (fig. S5C). In line with this finding, colocalization of mTOR and LAMP2
239 was enhanced in the sprouting front of $C2\beta^{KI/KI}$ retinas compared to that of control
240 littermates (Fig. 5C,D and fig. S5D). These findings are consistent with the observation
241 that activation of mTORC1 in wild-type retinas is more pronounced at the sprouting

242 front than in areas of remodeling (fig. S5E,F) (*23, 37, 38*). This spatial difference in
243 mTORC1 activation in C2$\beta^{KI/KI}$ retinas suggests that the PI3K-C2β/mTORC1 axis
244 primarily regulates cell growth in areas of prominent sprouting activity. To gain further
245 insight, we used EC-mTmG mice to label single cells and study the association
246 between mTORC1 activity and cell growth in a wild-type background. Given that the
247 phenotype of C2$\beta^{KI/KI}$ retinas commences at P6 and is followed by an enhanced cell
248 growth at P8 (Fig. 1B-D), we studied wild-type retinas in an intermediate time point
249 (P7). As we hypothesized, cell size and mTORC1 activity exhibited a positive
250 correlation, with larger cells being associated with higher p-S6 levels (Fig. 5E,F and
251 fig. S5G). We also observed that endothelial cells located at the sprouting front were
252 larger than cells located in remodeling areas (fig. S5H). Finally, suppression of
253 mTORC1 activity with rapamycin (Fig. 5G,H) resulted in normalization of the
254 exacerbated vessel enlargement and mTORC1 signaling of C2$\beta^{KI/KI}$ mice (Fig. 5G,I).
255 Together, these data demonstrate that PI3K-C2β signaling modulates mTORC1
256 activity in vivo and that aberrantly sustained mTORC1 activation promotes endothelial
257 cell growth during sprouting angiogenesis, primarily during early sprouting phases.
258 This agrees with the notion that cells located in sprouting areas show prominent
259 anabolic growth and active proliferation compared to those found in remodeling areas
260 (*27, 28, 37*).
261
262
263 **Discussion**
264 Understanding the molecular mechanisms that regulate endothelial cell
265 functions during vascular growth is essential to develop new anti-angiogenic
266 therapies. In our study, we identified a new player in the angiogenic cascade, namely
267 the class II PI3K isoform PI3K-C2β, which served as a negative regulator of
268 mTORC1/S6K1 signaling (Fig. 6). We found that this mTORC1/S6K1 regulation was
269 driven by the catalytic activity of PI3K-C2β, in line with data from Marat *et al.* who
270 showed that it is the local PIP_2 synthesis by PI3K-C2β that regulates cell growth in
271 HeLa cells (*15*). Here, we revealed that the suppression of mTORC1 by PI3K-
272 C2β occurred independently of the type of activating cue for mTORC1, although this
273 regulation appeared more prominent in response to growth factors. Previous in vitro
274 findings identify that PI3K-C2β–related regulation mainly occurs during growth factor

275 deprivation (*15*). Although our data are consistent with this finding, we found a more
276 pleiotropic role of PI3K-C2β-mediated regulation of mTORC1 encompassing both
277 starvation and in the presence of growth factor and nutrients. Considering that
278 endothelial cells represent the first regulatory interface for nutrient availability (*42*), it
279 is possible that they have developed a more finely tuned molecular machinery to
280 detect and react nutrient cues. Collectively, our data indicates that PI3K-C2β is a key
281 component in the regulation of mTORC1/S6K signaling pathway in endothelial cells,
282 specifically during angiogenesis and further supports the notion that endothelial cells
283 are exquisitely regulated by the activity of several class I and class II PI3K isoforms
284 (*4, 5*). Germline or somatic mutations in components of PI3K family are frequent in
285 congenital vascular disorders with mTOR signaling playing a central role in such
286 pathogenesis (*4*). Ultra-rare variants in *PIK3C2B* cause focal epilepsy in humans (*43*),
287 and based on our data, it is tempting to speculate that these patients also have a
288 predisposition to develop vascular anomalies, perhaps in an epistatic context. This
289 may be relevant to some patients with vascular malformations associated with high
290 PI3K/mTORC1 signaling for which the genetic cause is unknown (*4, 44, 45*).
291 mTORC1 signaling is required for vascular growth (*37, 45-47*). However, those
292 studies use either constitutive activation or full inhibition of mTORC1 signaling, with
293 both phenotypes leading to a profound dysregulation of cell proliferation. PI3K-C2β
294 inactivation resulted in a moderate increase in mTORC1 signaling which instead led
295 to a selective cell growth phenotype. However, it is not clear why proliferation in
296 endothelial cells is not perturbed by PI3K-C2β inactivation. One possibility is that the
297 threshold of mTORC1 activity required to engage into abnormal cell proliferation (*46*)
298 is not achieved by PI3K-C2β inactivation. However, it is also possible that PI3K-C2β
299 selectively regulates the growth response associated with mTORC1 signaling by
300 controlling mTORC1 location within the cell. Indeed, mTOR and LAMP2 overlapping
301 staining was increased in angiogenic endothelial cells located in the sprouting front of
302 C2β$^{KI/KI}$ P8 retinas which supports a model of regional regulation. This is consistent
303 with the observation that mTOR and LAMP2 co-localization was not increased in PI3K-
304 C2β null HUVECs because this model does not recapitulate various cellular states that
305 occur during angiogenesis. In line with spatiotemporal regulation of mTORC1
306 signaling, Ersching *et al.* have demonstrated that mTORC1 activation in vivo is
307 required for both cell growth at the light zone and cell proliferation at dark zone of B

308 cells in the germinal center, with these two events occurring in a sequential fashion
309 (*33*). Our results suggest a model in which activation of PI3K-C2β blocks
310 mTORC1/S6K1 signaling when endothelial cells have acquired the adequate cell size
311 to divide. Hence, when PI3K-C2β is inactivated, endothelial cells become larger as
312 result of persistent mTORC1 signaling over time. Also, our data further support a
313 model in which mTORC1-related regulation of cell growth and cell proliferation are
314 uncoupled, as previously shown in cultured cells (*48*). In line with this notion, it has
315 been recently shown that arteriovenous malformation are formed through mTORC1-
316 related increase in cell volume with minor contribution to cell proliferation (*49*).
317 The understanding of how class II PI3K isoforms function in vivo has remained
318 largely enigmatic. This is partially due to the notion that these enzymes do not act as
319 classical signal tranducers such as class I PI3Ks (*10*) but instead regulate the
320 trafficking of cellular membranes where signaling events occur. Our data strengthen
321 the concept that class II PI3Ks, and in particular PI3K-C2β, are also essential elements
322 in such signaling events, because disruption of its activity leads to profound alterations
323 in signaling also in vivo. An interesting observation extracted from our work is that
324 PI3K-C2β appears to regulate distinct signaling events based on the extracellular input
325 in vivo. Indeed, in response to insulin, PI3K-C2β modulates AKT activity in metabolic
326 tissues (*17*), whereas we showed that in response to angiogenic clues, such as
327 VEGFA, PI3K-C2β regulated mTORC1 activity independently of AKT. Collectively,
328 our results show that PI3K-C2β is a crucial determinant of endothelial signaling and
329 provide evidence of PI3K-C2β-dependent regulation of mTORC1 activity during
330 sprouting angiogenesis. We propose that acute targeting of PI3K-C2β may provide a
331 mean to restore endothelial mTORC1 activity in disease conditions.

332 **Materials and Methods**

333 ***Reagents***

334 All reagents were purchased from Sigma-Aldrich, unless stated otherwise. Media and
335 buffers for cell culture experiments were purchased from Lonza and Gibco. Primers
336 were obtained from Invitrogen.

337

338 ***Mice***

339 Animal experiments were performed in agreement with the guidelines and legislations
340 of the Catalan Ministry of Agriculture, Livestock, Fisheries and Food (Catalonia,
341 Spain), following protocols approved by the local Ethics Committees of IDIBELL-and
342 IGTP CEEAs. Mice were kept in individually ventilated cages under specific pathogen-
343 free conditions. All mice were crossed onto the C57BL/6J genetic background.
344 *Pik3c2b*$^{D1212A/D1212A}$ (referred to as C2β$^{KI/KI}$) mice carry constitutive inactivating point
345 mutations (D1212A) in the protein´s catalytic domain in both *Pik3c2b* alleles (*17*).
346 *Pik3c2b*$^{WT/WT}$ (referred to as C2β$^{WT/WT}$) mice were used as controls. ROSA-mTmG
347 double fluorescent reporter mice (*36*) were crossed onto *Pdgfb*-iCreER mice that
348 express an inducible iCreER recombinase from the endogenous *Pdgfb* locus (EC-
349 specific) (*35*). *Pdgfb*-iCreER:ROSA-mTmG mice were crossed onto C2β$^{KI/KI}$ animals.
350 C2β$^{WT/WT}$ mice crossed onto *Pdgfb*-iCreER:ROSA-mTmG were used as controls. A
351 single dose of 0.25 µg of 4-hydroxytamoxifen (4-OHT) was injected intraperitoneally
352 into postnatal day 6 (P6) mice to GFP label individual cells and retinas were isolated
353 on P8. Rapamycin (Sigma, R0395) was prepared at a concentration of 1.2 mg/ml in
354 DMSO. Pure DMSO was used as a vehicle control. Mice were injected
355 intraperitoneally for two consecutive days (P6 and P7) with 10 µl of rapamycin per
356 animal (3 mg/kg), and retinas were collected on P8 for immunostaining. 5-ethynyl-2'-
357 deoxyuridine (EdU)-incorporation assay was performed using a commercially
358 available kit (Invitrogen, C10340). Animals were injected intraperitoneally with 60 µl of
359 EdU (0.5 mg/ml in 50% DMSO and 50% PBS solution) and after 2 h the animals were
360 sacrificed and retinas were collected. EdU incorporation was detected with Click-iT
361 EdU Alexa Fluor-647 Imaging Kit, following the manufacturer's instructions. For other
362 types of immunostaining, the standard protocol in the next section was applied.

363

364 ***Mouse retina isolation and immunostaining***

365 Mice were culled by decapitation and eyes were enucleated and incubated on ice in
366 4% PFA for 1 hour. Isolated retinas were fixed in 4% PFA for an additional hour and
367 permeabilized overnight at 4°C in permeabilization/blocking buffer (1% BSA, 0.3%
368 Triton X-100 in PBS). Retinas were incubated overnight at 4°C with specific primary
369 antibodies diluted in permeabilization/blocking buffer (anti-Erg (Abcam, ab92513,
370 diluted 1:400, anti-GFP (Acris, R1091P, diluted 1:300), anti-phospho-HH3 (Millipore,
371 06-570, diluted 1:200), anti-p-S6 $Ser^{235/236}$ (Cell Signaling Technology, 4857, diluted
372 1:100), anti-p-S6 $Ser^{240/244}$ (Cell Signaling Technology, 2215S, diluted 1:100), anti-
373 LAMP2 (Santa Cruz, SC-18822, diluted 1:50), anti-mTOR (Cell Signaling Technology,
374 2983, diluted 1:500). Samples were washed three times in PBS containing 1% Tween-
375 20 (PBST), then incubated with PBLEC buffer (1% Triton X- 100, 1 mM $CaCl_2$, 1 mM
376 $MgCl_2$ and 1 mM $MnCl_2$ in PBS, pH 6.8) for 30 min at room temperature. Secondary
377 Alexa Fluor-conjugated antibodies diluted in PBLEC were added to the retinas and
378 incubated for another 2 h at room temperature (Invitrogen, A11001, A11011, A11008,
379 A31573). Blood vessels were visualized with Alexa Fluor-conjugated isolectin GS-B4
380 (Molecular Probes, I21411, I21412). Following three washes with PBST, the tissues
381 were flat mounted on a microscope slide.
382
383 ***Confocal imaging and image quantification***
384 Imaging was performed with a Leica TCS SP5 confocal microscope and with a Leica
385 Stellaris 8. Volocity, Adobe Photoshop 2022 and ImageJ software were used for image
386 editing and quantification, respectively. Images were taken from at least 5 retinal areas
387 in each mouse and at least three mice per genotype were analyzed. Retina vascularity
388 was measured using the IB4 channel by adjusting the threshold to select the IB4-
389 positive area, which was quantified by dividing the percentage of IB4-positive area by
390 the total image area (10^4 μm^2). The vessel width (μm) was determined manually from
391 10^4 μm^2 images using a proper scale setup. The number of vessel sprouts seen
392 throughout the sprouting front were calculated manually using the IB4 channel. The
393 length of the sprouting front was measured manually. The data were presented as the
394 number of sprouts per 100 μm of the sprouting front. The EC number was determined
395 manually based on EC-specific nuclei staining (Erg) per 10^4 μm^2 image area.
396 Quantification of EC proliferation was performed using EdU or pHH3 and Erg co-
397 immunostaining and both EdU or pHH3- and Erg-positive ECs were quantified in a 10^4
398 μm^2 image area. The vascular-specific p-S6 intensity was measured using both the p-

399 S6 and IB4 channels. First, a manual threshold was set to obtain the IB4-positive area
400 that served as an IB4 mask and to define the region of interest (ROI). Then, using the
401 defined IB4 mask, the integrated p-S6 density was measured only in IB4-positive
402 areas. The background measurements (mean gray values) were taken from areas in
403 close proximity to the vasculature but that were negative for IB4. To correct for
404 measured area and staining background, the corrected total fluorescence (CTF) was
405 calculated based on the following equation: CTF = integrated density – (vascular area
406 × mean gray background value). Endothelial cell area was determined by using EC-
407 mTmG mouse line. The area of individual GFP-positive endothelial cells in the
408 sprouting front was measured in both C2β$^{WT/WT}$ and C2β$^{KI/KI}$ animals. Lysosomal
409 mTOR was represented as the percentage of double mTOR- and LAMP2-positive
410 vesicles of the total vesicular mTOR in IB4^{+} endothelial cells in the sprouting front.
411
412 ***siRNA-mediated knockdown of PIK3C2B in HUVECs***
413 HUVECs were purchased from Lonza (#C2519A) and cultured in 0.5% gelatin-coated
414 plates in EBM-2 supplemented with EGM-2 BulletKit (Lonza, #CC-3162), 10% FBS
415 and 1% penicillin/streptomycin, referred to as EGM-2 complete. Cells were cultured
416 until passage six. $0.3 \cdot 10^5$ HUVECs were seeded onto 0.5% gelatin-coated wells (in a
417 6-well format) and cultured overnight at 37°C in 5% CO_2 atmosphere. The next day,
418 cells were transfected with two different siRNAs against PI3K-C2β using
419 Lipofectamine® RNAiMAX (Invitrogen,13778075) according to the manufacture´s
420 protocol. Scrambled (nontargeting) oligonucleotide was used as a control. Briefly, 2 µl
421 of each oligonucleotide (100 µM) were diluted in 200 µl of OptiMEM. Similarly, 4 µl of
422 Lipofectamine® RNAiMAX were diluted in 200 µl of OptiMEM. The tubes were
423 incubated for 5 min, mixed thoroughly together, and incubated at room temperature
424 for 25 min. The culture medium has been changed for a complete EGM-2 deprived
425 from penicillin/streptomycin and heparin. The transfection solution was added
426 dropwise onto the cells and incubated for 5-6 h. Cells were refreshed with complete
427 EGM-2 medium and cultured for an additional 48-72 h. Prior to further experiments,
428 cells were reseeded onto 0.5% gelatin-coated dishes. The following human-specific
429 siRNA sequences were used: scrambled: GUAACUGUCGGCUCGUGGU[dT][dT],
430 *PIK3C2B* #1: GUUCGACACUUACCACAAU-[dT][dT]. For experiments using
431 rapamycin, HUVECs were refreshed for 1 h with fresh EGM-2 complete medium, then
432 treated with 20 nM rapamycin (dissolved in DMSO). DMSO-treated cells were used

433 as controls. After 6 h incubation, protein lysates were obtained and kept at -80°C for
434 future analysis.
435
436 ***Primary mouse lung endothelial cell (MLEC) isolation and culture***
437 MLECs were isolated from adult C57Bl6/J mice, including females and males,
438 between 3- and 6-week-old. Briefly, lungs were homogenized with a scalpel blade and
439 incubated in dispase II (Gibco, #17105-041) in Hank's Balanced Salt Solution (4 U/ml)
440 for 1 h at 37°C. The digested tissue was disintegrated by pipetting into a single-cell
441 solution, and enzyme was inactivated with DMEM supplemented with 10% FBS and
442 1% penicillin/streptomycin. Cells were resuspended in PBS and incubated with rat
443 anti-CD144 antibody-coated magnetic beads for 30 min at room temperature. The
444 CD144-positive fraction was washed with PBS with 0.5% BSA and sorted using a
445 magnet. Cells were resuspended and cultured in 0.5% gelatin-coated culture wells (in
446 a 12-well format) in F12/DMEM medium supplemented with 20% FBS, 1%
447 penicillin/streptomycin and 4 ml endothelial cell growth factors, referred to as F12
448 complete (PromoCell, #C30140), until they reached 80-90% confluency. Cells were
449 subjected to a second selection with the CD144 antibody-coated magnetic beads for
450 1 h at room temperature, then trypsinized, magnet-sorted, resuspended in F12
451 complete medium and further cultured (in a 6-well format). Cells were cultured at 37°C
452 in 5% CO_2 atmosphere and used for experiments until passage 5.
453
454 ***Cell size analysis by flow cytometry***
455 Cells were trypsinized for 5 min, and trypsin was neutralized with DMEM containing
456 10% FBS and 1% penicillin/streptomycin. Cells were centrifuged at 300g for 5 min.
457 Cells were washed twice with cold PBS and the cell pellet was resuspended in 300 µl
458 of FACS buffer (0.1% BSA, 3 mM EDTA in PBS). 100 µl of 1X DAPI (Sigma, D9542)
459 was added to the samples and cells were analyzed on BD FACSCanto™ II. Results
460 were analyzed with the FlowJo software.
461
462 ***BrdU and EdU proliferation assay in vitro***
463 5-ethynyl-2'-deoxyuridine (EdU) (Invitrogen, C10340) incorporation and 5-bromo-2
464 deoxyuridine (BrdU) assays were used to analyze cell proliferation. Cells were
465 incubated with 20 µM of EdU or BrdU (Sigma, B5002) for 2 h. Cells were fixed with
466 4% PFA for 15 min, blocked with 3% BSA in PBS for 30 min, and stained with EdU

467 and BrdU. 5 min incubation with DAPI was used to stain nuclei. 20X images were
468 taken using a confocal microscope and proliferating cells were manually counted and
469 graphically represented as a percentage over the total number of cells.
470
471 ***Wound healing assay***
472 $0.25x10^5$ cells were seeded onto a 0.5% gelatin-coated plate (in a 12-well format) and
473 cultured at 37°C in 5% CO_2 atmosphere until confluency. Prior to the experiment, cells
474 were incubated for 30 min with 1 µg/ml mitomycin C to inhibit cell proliferation. The
475 scratch was made using a pipette tip and brightfield images taken at 3 time points: T0
476 (reference point), T7 and T24. Both control- and PI3K-C2β–depleted cells exhibited
477 similar confluency before the scratch. Data were presented as the percentage of the
478 wound area.
479
480 ***Cell immunofluorescence***
481 Cells were seeded on gelatin-coated coverslips to reach sub- or full confluency the
482 next day and incubated overnight at 37°C in 5% CO_2 atmosphere. Cells were fixed
483 with 4% PFA for 15 min and washed three times with PBS. Cells were permeabilized
484 with 0.1% Triton X-100 in PBS (PBST) for 30 min and blocked with 3% BSA in PBS
485 for 1 h at room temperature. Cells were incubated with specific primary antibodies in
486 a blocking buffer at 4°C overnight. The following antibodies were used: anti-β-catenin
487 (BD Biosciences, 610153, diluted 1:200), anti-LAMP2 (Santa Cruz, SC-18822, diluted
488 1:50), anti-mTOR (Cell Signaling Technology, 2983, diluted 1:500). The next day, the
489 coverslips were washed 3 times with PBST, then incubated with secondary Alexa
490 Fluor-conjugated antibodies diluted in PBS 1:300 for 1 hour (Invitrogen, A11001,
491 A11011, A11008, A31573). After three washes with PBST, coverslips were mounted
492 on a microscope slide in a mounting medium (ThermoFisher Scientific, 9990402).
493 TOR and LAMP2 correlative co-staining were measured using Image J. To quantify
494 the subcellular distribution of lysosomal vesicles in cultured endothelial cells, we
495 designated those in the 1.5X area from the nuclear perimeter as "perinuclear" and
496 those that were in the 1.5X to 2X area from the nuclear perimeter as "peripheral". The
497 data show the percentage of LAMP2 vesicles that are present in either compartment.
498
499 ***Amino acid and growth factor deprivation***

500 $3.5 \cdot x10^5$ cells were seeded onto 0.5% gelatin-coated plates (in a 6-well format) and
501 cultured at 37°C in a 5% CO_2 atmosphere. First, cells were set up to start from identical
502 conditions. In each case, the medium was replaced by fresh EGM-2 complete medium
503 for 1 h. Cells were deprived of growth factors or amino acids for defined times after
504 which they were re-stimulated with 1% iFBS (ThermoFischer-LIFE Technologies,
505 10270) or with 1X amino acid set to see the differences in phosphorylated proteins
506 caused by this stimulation and the general response of cells in terms of the PI3K-
507 mTOR pathway. Two washes with PBS containing Ca^{2+} and Mg^{2+} ions were performed
508 before lysing cells for further analysis.
509
510 ***VEGF stimulation experiment***
511 $0.3x10^5$ HUVECs were seeded onto 0.5% gelatin-coated wells (in a 6-well format) and
512 cultured overnight at 37°C in 5% CO2 atmosphere. The next day, cells were washed
513 twice with PBS containing Ca^{2+} and Mg^{2+} ions, serum-starved for 4 h, and stimulated
514 with 100 ng/ml recombinant human VEGF-A (R&D Systems, 293-VE) or 1% FBS for
515 15 minutes. Cells were starved in EBM-2 basal medium (without supplements).
516 Stimulating agents were diluted in EBM-2 basal medium. Cells were washed
517 immediately with cold PBS and lysed for protein extraction. Serum-starved, non-
518 stimulated cells were used as a control.
519
520 ***Protein extraction and immunoblotting***
521 Cells were lysed in ice cold lysis buffer (50 mM Tris-HCl pH 7.4, 5 mM EDTA, 150 mM
522 NaCl and 1% Triton X-100 supplemented with 2 mg/ml aprotinin, 1 mM sodium
523 fluoride, 1 mM pepstatin, 1 ng/ml leupeptin, 1 mM phenylmethanesulfonyl fluoride
524 (PMSF), 10 g/ml Nα-tosyl-L-lysine chloromethyl ketone hydrochloride (TLCK), 1 mM
525 sodium orthovanadate, 1 μM okadaic acid and 1 mM dithiothreitol) for 15 min then
526 centrifuged at >16000 g for 15 min at 4°C. Protein concentrations of the supernatants
527 were measured with the Pierce BCA Protein Assay Kit (Thermo Fisher Scientific,
528 23225) following the manufacturer's instructions. Total cell lysates were resolved on
529 8% or 10% SDS-containing polyacrylamide gels and transferred onto nitrocellulose
530 membranes (Pall Corporation, 66485) for 2 h at 250 mA. The membranes were
531 blocked in 5% milk in TBST (TBS buffer with 0.1% Tween 20) for 1 hm, then incubated
532 overnight with the following specific primary antibodies diluted in 2% BSA in TBS-T:
533 anti-PI3K-C2β (BD Biosciences, 611343, diluted 1:500), anti-p-AKT (Ser^{473}) (Cell

534 Signaling Technology, 4060, diluted 1:1000), anti-AKT (Cell Signaling Technology,
535 9272, diluted 1:1000), anti-p-S6(S235/236) (Cell Signaling Technology, 4857, diluted
536 1:1000), anti-p-S6 ($Ser^{240/244}$) (Cell Signaling Technology, 2215S, diluted 1:1000), anti-
537 S6 (Cell Signaling Technology, 2217, diluted 1:1000), anti-p-S6K (Thr^{389}) (Cell
538 Signaling Technology, 9234, diluted 1:500), anti-S6K (Cell Signaling Technology,
539 2708, diluted 1:1000), anti-vinculin (Abcam, ab49900, diluted 1:10000), anti-β-actin
540 (Sigma, A5441, diluted 1:10000). After three washes in TBST, the membranes were
541 incubated with the appropriate horseradish peroxidase (HRP)-conjugated secondary
542 antibody, washed 5 times in TBST and developed with reagents for enhanced
543 chemiluminescence. The following secondary antibodies from DAKO were used (all
544 diluted 1:5000): pig anti-rabbit (P0399), rabbit anti-goat (P0449), rabbit anti-mouse
545 (P0260), and rabbit anti-sheep (P0163). All immunoblots were performed at least 3
546 times independently, and representative experiments were included in the figures.
547 Quantifications were done using ImageJ.
548
549 ***Statistics***
550 Each scientific question in which statistical analysis was performed was addressed in
551 a pilot experiment using n=3 per group or based on similar previously published
552 experiments. With these results, power analysis on these preliminary data was
553 performed, suggesting a minimal cohort size of 3-6 to see a medium difference with
554 80% power, depending on the type of experiment. The sample size for each
555 experiment is indicated in the corresponding figure legend. No blinding was
556 performed. Genotypes were not known at the time of treatment or immunostaining.
557 Statistical analysis was determined by a two-tailed or one-tailed Mann-Whitney test
558 using GraphPad Prism 9 (GraphPad Software Inc.). All figures are displayed with
559 individual data points that indicate biological replicates and with the standard error of
560 the mean (s.e.m.) as errors bars. At least 3 biological replicates were used. P values
561 considered as statistically significant were as follows: $*p \leq 0.05$; $**p \leq 0.01$, $***p \leq$
562 0.001 and $****p \leq 0.0001$.

Supplementary Materials

Figs. S1-S5.

567 **References and Notes**
568

569 1. M. Potente, T. Makinen, Vascular heterogeneity and specialization in
570 development and disease. *Nat Rev Mol Cell Biol* **18**, 477-494 (2017).
571 2. P. Carmeliet, Blood vessels and nerves: common signals, pathways and
572 diseases. *Nat Rev Genet* **4**, 710-720 (2003).
573 3. E. Trimm, K. Red-Horse, Vascular endothelial cell development and diversity.
574 *Nat Rev Cardiol*, (2022).
575 4. A. Angulo-Urarte, M. Graupera, When, where and which PIK3CA mutations are
576 pathogenic in congenital disorders. *Nature Cardiovascular Research* **1**, 700-
577 714 (2022).
578 5. P. Kobialka, M. Graupera, Revisiting PI3-kinase signalling in angiogenesis.
579 *Vasc Biol* **1**, H125-H134 (2019).
580 6. M. Potente, H. Gerhardt, P. Carmeliet, Basic and therapeutic aspects of
581 angiogenesis. *Cell* **146**, 873-887 (2011).
582 7. C. A. Franco *et al.*, Dynamic endothelial cell rearrangements drive
583 developmental vessel regression. *PLoS Biol* **13**, e1002125 (2015).
584 8. B. Vanhaesebroeck, J. Guillermet-Guibert, M. Graupera, B. Bilanges, The
585 emerging mechanisms of isoform-specific PI3K signalling. *Nat Rev Mol Cell*
586 *Biol* **11**, 329-341 (2010).
587 9. D. A. Fruman *et al.*, The PI3K Pathway in Human Disease. *Cell* **170**, 605-635
588 (2017).
589 10. B. Bilanges, Y. Posor, B. Vanhaesebroeck, PI3K isoforms in cell signalling and
590 vesicle trafficking. *Nat Rev Mol Cell Biol* **20**, 515-534 (2019).
591 11. F. Gulluni, M. C. De Santis, J. P. Margaria, M. Martini, E. Hirsch, Class II PI3K
592 Functions in Cell Biology and Disease. *Trends Cell Biol* **29**, 339-359 (2019).
593 12. Y. Posor *et al.*, Spatiotemporal control of endocytosis by phosphatidylinositol-
594 3,4-bisphosphate. *Nature* **499**, 233-237 (2013).
595 13. I. Franco *et al.*, PI3K class II alpha controls spatially restricted endosomal
596 PtdIns3P and Rab11 activation to promote primary cilium function. *Dev Cell* **28**,
597 647-658 (2014).
598 14. C. C. Campa *et al.*, Rab11 activity and PtdIns(3)P turnover removes recycling
599 cargo from endosomes. *Nat Chem Biol* **14**, 801-810 (2018).
600 15. A. L. Marat *et al.*, mTORC1 activity repression by late endosomal
601 phosphatidylinositol 3,4-bisphosphate. *Science* **356**, 968-972 (2017).
602 16. Y. Posor *et al.*, Local synthesis of the phosphatidylinositol-3,4-bisphosphate
603 lipid drives focal adhesion turnover. *Dev Cell* **57**, 1694-1711 e1697 (2022).
604 17. S. Alliouachene *et al.*, Inactivation of the Class II PI3K-C2beta Potentiates
605 Insulin Signaling and Sensitivity. *Cell Rep* **13**, 1881-1894 (2015).
606 18. M. Graupera *et al.*, Angiogenesis selectively requires the p110alpha isoform of
607 PI3K to control endothelial cell migration. *Nature* **453**, 662-666 (2008).
608 19. A. Angulo-Urarte *et al.*, Endothelial cell rearrangements during vascular
609 patterning require PI3-kinase-mediated inhibition of actomyosin contractility.
610 *Nat Commun* **9**, 4826 (2018).

611 20. K. Yoshioka *et al.*, Endothelial PI3K-C2alpha, a class II PI3K, has an essential
612 role in angiogenesis and vascular barrier function. *Nat Med* **18**, 1560-1569
613 (2012).
614 21. T. Anquetil *et al.*, PI3KC2beta inactivation stabilizes VE-cadherin junctions and
615 preserves vascular integrity. *EMBO Rep* **22**, e51299 (2021).
616 22. G. Tibolla *et al.*, Class II phosphoinositide 3-kinases contribute to endothelial
617 cells morphogenesis. *PLoS One* **8**, e53808 (2013).
618 23. A. M. Figueiredo *et al.*, Phosphoinositide 3-Kinase-Regulated Pericyte
619 Maturation Governs Vascular Remodeling. *Circulation* **142**, 688-704 (2020).
620 24. M. E. Pitulescu, I. Schmidt, R. Benedito, R. H. Adams, Inducible gene targeting
621 in the neonatal vasculature and analysis of retinal angiogenesis in mice. *Nat*
622 *Protoc* **5**, 1518-1534 (2010).
623 25. P. Kobialka *et al.*, The onset of PI3K-related vascular malformations occurs
624 during angiogenesis and is prevented by the AKT inhibitor miransertib. *EMBO*
625 *Mol Med* **14**, e15619 (2022).
626 26. N. W. Chavkin *et al.*, Endothelial cell cycle state determines propensity for
627 arterial-venous fate. *Nat Commun* **13**, 5891 (2022).
628 27. H. Serra *et al.*, PTEN mediates Notch-dependent stalk cell arrest in
629 angiogenesis. *Nat Commun* **6**, 7935 (2015).
630 28. K. Wilhelm *et al.*, FOXO1 couples metabolic activity and growth state in the
631 vascular endothelium. *Nature* **529**, 216-220 (2016).
632 29. M. Castro *et al.*, CDC42 Deletion Elicits Cerebral Vascular Malformations via
633 Increased MEKK3-Dependent KLF4 Expression. *Circ Res* **124**, 1240-1252
634 (2019).
635 30. J. Bernier-Latmani *et al.*, Apelin-driven endothelial cell migration sustains
636 intestinal progenitor cells and tumor growth. *Nat Cardiovasc Res* **1**, 476-490
637 (2022).
638 31. S. Muhleder, M. Fernandez-Chacon, I. Garcia-Gonzalez, R. Benedito,
639 Endothelial sprouting, proliferation, or senescence: tipping the balance from
640 physiology to pathology. *Cell Mol Life Sci* **78**, 1329-1354 (2021).
641 32. G. Y. Liu, D. M. Sabatini, mTOR at the nexus of nutrition, growth, ageing and
642 disease. *Nat Rev Mol Cell Biol* **21**, 183-203 (2020).
643 33. J. Ersching *et al.*, Germinal Center Selection and Affinity Maturation Require
644 Dynamic Regulation of mTORC1 Kinase. *Immunity* **46**, 1045-1058 e1046
645 (2017).
646 34. A. Wallroth, P. A. Koch, A. L. Marat, E. Krause, V. Haucke, Protein kinase N
647 controls a lysosomal lipid switch to facilitate nutrient signalling via mTORC1.
648 *Nat Cell Biol* **21**, 1093-1101 (2019).
649 35. S. Claxton *et al.*, Efficient, inducible Cre-recombinase activation in vascular
650 endothelium. *Genesis* **46**, 74-80 (2008).
651 36. M. D. Muzumdar, B. Tasic, K. Miyamichi, L. Li, L. Luo, A global double-
652 fluorescent Cre reporter mouse. *Genesis* **45**, 593-605 (2007).
653 37. Y. T. Ong *et al.*, A YAP/TAZ-TEAD signalling module links endothelial nutrient
654 acquisition to angiogenic growth. *Nat Metab* **4**, 672-682 (2022).

38. R. E. Oberkersch *et al.*, Aspartate metabolism in endothelial cells activates the mTORC1 pathway to initiate translation during angiogenesis. *Dev Cell* **57**, 1241-1256 e1248 (2022).
39. V. I. Korolchuk *et al.*, Lysosomal positioning coordinates cellular nutrient responses. *Nat Cell Biol* **13**, 453-460 (2011).
40. A. Efeyan, D. M. Sabatini, Nutrients and growth factors in mTORC1 activation. *Biochem Soc Trans* **41**, 902-905 (2013).
41. A. Ortega-Molina *et al.*, Oncogenic Rag GTPase signaling enhances B cell activation and drives follicular lymphoma sensitive to pharmacological inhibition of mTOR. *Nat Metab* **1**, 775-789 (2019).
42. M. Graupera, M. Claret, Endothelial Cells: New Players in Obesity and Related Metabolic Disorders. *Trends Endocrinol Metab* **29**, 781-794 (2018).
43. L. Gozzelino *et al.*, Defective lipid signalling caused by mutations in PIK3C2B underlies focal epilepsy. *Brain* **145**, 2313-2331 (2022).
44. W. Y. Aw *et al.*, Microphysiological model of PIK3CA-driven vascular malformations reveals a role of dysregulated Rac1 and mTORC1/2 in lesion formation. *Sci Adv* **9**, eade8939 (2023).
45. S. Wang *et al.*, Regulation of endothelial cell proliferation and vascular assembly through distinct mTORC2 signaling pathways. *Mol Cell Biol* **35**, 1299-1313 (2015).
46. S. Sun *et al.*, Constitutive Activation of mTORC1 in Endothelial Cells Leads to the Development and Progression of Lymphangiosarcoma through VEGF Autocrine Signaling. *Cancer Cell* **28**, 758-772 (2015).
47. T. L. Phung *et al.*, Pathological angiogenesis is induced by sustained Akt signaling and inhibited by rapamycin. *Cancer Cell* **10**, 159-170 (2006).
48. R. J. Dowling *et al.*, mTORC1-mediated cell proliferation, but not cell growth, controlled by the 4E-BPs. *Science* **328**, 1172-1176 (2010).
49. M. P. Ouarne, A.; Ramalho, D.; Conchinha, N.V.; Costa, T.; Figueiredo, A.; Pimentel Saraiva, M.; Carvalho, Y.; henado Misikonva, L.; Oh P.S., Franco, C.A., A non-genetic model of vascular shunts informs on the cellular1mechanisms of formation and resolution of arteriovenous2malformations. *bioRxiv*, (2023).

Acknowledgments

We thank members of the Endothelial Pathobiology and Microenvironment Group for helpful discussions.

Funding

We thank CERCA Program/Generalitat de Catalunya and the Josep Carreras Foundation for institutional support. This publication is part of the R+D+€ project PID2020-116184RB-I00 funded by MCIN/ AEI/10.13039/501100011033. M.G. laboratory is also supported by the following research grants: the Excellence Network Grant from MICIU/AEI (SAF2016-81975-REDT, also to A.E.); PTEN RESEARCH Foundation (IJC-21-001); la Caixa Banking Foundation (LCF/PR/HR21/00046, also to A.E.); by la Asociación Española contra el Cancer (AECC)-Grupos Traslacionales (GCTRA18006CARR); by la Fundación BBVA (Ayuda Fundación BBVA a Equipos de Investigación Científica 2019, PR(19)BIO_MET_0061); World Cancer Research (21-0159). A.E. laboratory is founded by MICINN (PID2019-104012RB-I00). The work of MP was supported by the European Research Council (ERC) Consolidator Grant EMERGE (no. 773047). Personal support was from Marie-Curie ITN Actions (P.K.) grant agreement 675392. S.D.C. is funded by la Caixa Banking Foundation Junior Leader project (LCF/BQ/PR20/11770002). A.A-U is a recipient of a fellowship from the European Union's Horizon 2020 Research and Innovation Programme under the Marie Sklodowska-Curie grant agreement No 101026227.

Authors contributions: P.K., J.LL., A.E., and M.G. designed research; P.K., J.LL., N. D-S., M.M., P.V., L.M., J.A., A. A-U., S.D.C., J.A.D., H.v.S., A. A., J.G-B. performed research; P.K., J.LL., N. D-S., J.G-B., A.E., and M.G. analyzed data; B.V. and M.P. contributed new reagents; P.K., J.LL., A.E., M.G. wrote the paper.

Competing interests: B.V. is a consultant for iOnctura (Geneva, Switzerland), Venthera (Palo Alto, US), Pharming (Leiden, the Netherlands) and Olema Pharmaceuticals (San Francisco, US). The other authors declare that they have no competing interests.

Data and materials availability: All data needed to evaluate the conclusions in the paper are present in the paper or the Supplementary Materials.

722 **Figure 1. Inactivation of PI3K-C2β results in enlarged blood vascular tubes**
723 **during angiogenesis.**
724 (**A**) Schematic of PI3K-C2β kinase-dead protein variant highlighting the D1212A point
725 mutation in the catalytic domain.
726 (**B**) Representative images of control ($C2\beta^{WT/WT}$) and $C2\beta^{KI/KI}$ retinas isolated at three
727 developmental time points (P3, P6 and P8) and stained for blood vessels (isolectin B4
728 (IB4), grey). Upper panels show an overview of the retinal vasculature (scale bars:
729 150 μm). Lower panels show higher magnification of the retinal front areas from the
730 upper panel (scale bars: 30 μm).
731 (**C-D**) Quantification of vessel width (**C**) and vascular density (**D**). n ≥4 retinas from n
732 ≥3 mice per genotype.
733 (**E**) Representative sprouting front images taken from arterial and venous areas of P8
734 retinas isolated from control and $C2\beta^{KI/KI}$ mice. Vessels are labeled with IB4 (grey).
735 Scale bars: 30 μm.
736 (**F**) Quantification of vascular density by IB4-positive area in arterial and venous areas.
737 n=6 retinas from n ≥3 mice per genotype.
738 (**G**) Representative sprouting front images of P8 retinas isolated from control and
739 $C2\beta^{KI/KI}$ mice and immunostained for endothelial cell nuclei (Erg, cyan), proliferative
740 cells (EdU, magenta) and blood vessels (IB4, red). Yellow circles highlight proliferating
741 endothelial cells (both EdU- and Erg-positive). Scale bars: 30 μm.
742 (**H**) Quantification of the percentage of EdU/Erg ratio in control and $C2\beta^{KI/KI}$ retinas.
743 N=5 retinas from n ≥3 mice per genotype.
744 (**I**) Representative images of the sprouting front of P8 retinas immunostained for Erg
745 (black) to visualize endothelial cell nuclei. Scale bars: 30 μm.
746 (**J**) Quantification of the number of endothelial cells normalized to 10^4 μm^2 IB4-positive
747 area. n=6 retinas from n ≥3 mice per genotype.
748 All error bars are s.e.m. Statistical analysis was performed by two-tailed Mann-
749 Whitney test. *$p \leq 0.05$ and **$p \leq 0.01$.
750
751 **Figure 2. PI3K-C2β regulates endothelial cell growth.**
752 (**A**) Representative immunoblot showing efficiency of PI3K-C2β knockdown by siRNA
753 in HUVECs. Scrambled siRNA-treated HUVECs were used as a control.

754 (**B**) Quantification of PI3K-C2β levels normalized to β-actin levels. N=5 biological
755 replicates per group.
756 (**C**) Representative images of HUVECs transfected with scrambled and C2β-specific
757 siRNA and incubated with EdU (green) to label proliferative cells and with DAPI to
758 visualize cell nuclei. Scale bars: 80 μm.
759 (**D**) Quantification of the percentage of $EdU^+/DAPI^+$ cells. n=5 biological replicates per
760 group.
761 (**E**) Representative images of control and C2β-deficient HUVECs in a wound healing
762 assay. Images were taken at the starting point (T0), 7 and 24 h later. White dashed
763 lines show the borders of the wound. Scale bars: 1000 μm.
764 (**F**) Quantification of the percentage of the wound area relative to the starting point of
765 the corresponding group. n=3 biological replicates per group.
766 (**G**) Representative images of scrambled and C2β siRNA-transfected HUVECs in a
767 confluent state, stained for β-catenin to mark cell bodies. Scale bars: 20 μm.
768 (**H**) Quantification of cell area. n ≥95 cells per group from 3 independent experiments.
769 (**I**) Representative images of scrambled and C2β siRNA-transfected HUVECs in a
770 subconfluent (sparse) state, stained for paxillin to label focal adhesions. Scale bars:
771 20 μm.
772 (**J**) Quantification of cell area. n ≥130 cells per group from 3 independent experiments.
773 (**K**) Schematic illustrating the genetic strategy for endothelial cell labelling using
774 mTmG reporter mice (EC-mTmG). Following 4-hydroxytamoxifen administration, iCre-
775 ER recombinase specifically induces the expression of membrane-localized EGFP
776 (mG) in endothelial cells.
777 (**L**) Representative sprouting front images of P8 control and $C2\beta^{KIKI}$ EC-mTmG retinas
778 showing individually labelled endothelial cells (cyan). Blood vessel labeled by IB4
779 (red). Yellow dashed lines mark single endothelial cells. Scale bars: 10 μm.
780 (**M**) Quantification of cell size of individual endothelial cells. n ≥133 cells from n ≥6
781 independent retinas per genotype.
782 All error bars are s.e.m. Statistical analysis was performed by two-tailed Mann-
783 Whitney test. ***$p \leq 0.001$ and **$p \leq 0.0001$.
784
785 **Figure 3. PI3K-C2β limits mTORC1 signaling in endothelial cells.**

786 (**A**) Representative immunoblot of control and C2β-deficient HUVECs showing
787 activation of the mTORC1 pathway by assessing p-S6K-Thr^{389} and p-S6-Ser$^{235/236}$
788 levels.
789 (**B**) Quantification of p-AKT-Ser^{473}, p-S6K-Thr^{389} and p-S6-Ser$^{235/236}$ levels normalized
790 to total vinculin. Graphs show the mean of 5 biological replicates per group.
791 (**C**) Immunoblot showing the impact of rapamycin on mTORC1 signaling in scramble-
792 and siRNA-treated HUVECs.
793 (**D**) Quantification of p-S6K-Thr^{389} and p-S6-Ser$^{235/236}$ levels normalized to vinculin
794 levels. n=4 biological replicates per group.
795 (**E**) Representative confocal images of control and C2β-depleted HUVECs
796 immunostained for mTOR (cyan) and the lysosomal marker LAMP2 (magenta). Yellow
797 rectangles show higher magnification of individual cells. Scale bar, 20μm.
798 (**F-H**) Quantification of the Pearson correlation analysis of mTOR and LAMP2 staining
799 (**F**), the percentage of the peripheral (**G**) and perinuclear (**H**) mTOR-LAMP2
800 complexes. n ≥17 (**F**) and n=62 cells (control) and 90 cells (C2β siRNA-treated) (**G**
801 **and H**). Data from 2 independent experiments.
802 All error bars are s.e.m. Statistical analysis was performed by one-tailed (**B,D**) and
803 two-tailed (**F-H**) Mann-Whitney test. ** $p \leq 0.01$ and ****$p \leq 0.0001$.
804
805 **Figure 4. The impact of growth factors and amino acids on PI3K-C2β-mediated**
806 **mTORC1 signaling.**
807 (**A**) Immunoblot showing the impact of growth factor deprivation on
808 PI3K/AKT/mTORC1 activity in control and C2β-deficient HUVECs in a time-dependent
809 manner.
810 (**B**) Quantification of p-S6K-Thr^{389} and p-S6-Ser$^{235/236}$ levels normalized to vinculin
811 levels. Graphs show the mean of n ≥4 biological replicates per group.
812 (**C**) Immunoblot showing the impact of amino acid deprivation on PI3K/AKT/mTORC1
813 activity in control and C2β siRNA-transfected HUVECs in a time-dependent manner.
814 (**D**) Quantification of p-S6K-Thr^{389} and p-S6-Ser$^{235/236}$ levels normalized to total
815 vinculin levels. Graphs show the mean of n=4 biological replicates per group.
816 (**E**) Representative immunoblot showing the effect of growth factor stimulation on
817 PI3K/AKT/mTORC1 activity in control and C2β-deficient HUVECs.

818 (**F**) Quantification of p-S6K-Thr^{389} and p-S6-Ser$^{235/236}$ levels normalized to vinculin
819 levels, respectively. Graphs show the mean of n=5 biological replicates per group.
820 (**G**) Representative immunoblot showing the impact of stimulation with amino acids on
821 PI3K/AKT/mTORC1 signaling in control and C2β-deficient HUVECs.
822 (**H**) Quantification of p-S6K-Thr^{389} and p-S6-Ser$^{235/236}$ levels normalized to vinculin
823 levels, respectively. Graphs show the mean of n=6 biological replicates per group.
824 All error bars are s.e.m. Statistical analysis was performed by one-tailed Mann-
825 Whitney test. *p ≤ 0.05 and **p ≤ 0.01.
826
827 **Figure 5. PI3K-C2β inactivation leads to elevated mTORC1 signaling during**
828 **angiogenesis.**
829 (**A**) Representative sprouting front images of P6 retinas isolated from control and
830 C2β$^{KI/KI}$ mice, followed by immunostaining for p-S6-Ser$^{235/236}$; white). Blood vessels
831 stained with IB4 (red). Scale bars: 30 μm.
832 (**B**) Quantification of p-S6-Ser$^{235/236}$ intensity in blood vessels. n ≥4 retinas from n ≥3
833 mice per genotype.
834 (**C**) Representative sprouting front images of P8 retinas isolated from control and
835 C2β$^{KI/KI}$ mice, followed by immunostaining for mTOR (cyan), LAMP2 (red). Blood
836 vessels stained with IB4 (white). Upper panels show an overview of the retinal
837 vasculature (scale bars: 30 μm). Lower panels show higher magnification of the retinal
838 front areas from the upper panel (scale bars: 5 μm). Arrows show overlapping mTOR
839 and LAMPs co-staining
840 (**D**) Quantification of % of mTOR and LAMP2 co-localization within the IB4 positive
841 area. n=20 cells from 4 mice per genotype.
842 (**E**) Representative images of sprouting front and remodeling plexus from P7 EC-
843 mTmG retinas immunostained for p-S6-Ser$^{235/236}$ (white). Blood vessels were
844 visualized with IB4 (blue), with individually GFP-labelled endothelial cells (green).
845 Yellow dashed lines outline single endothelial cells. Scale bars: 10 μm.
846 (**F**) Correlation analysis between endothelial cell size and p-S6-Ser$^{235/236}$ level in the
847 sprouting front and remodeling plexus. n=131 cells (sprouting front) and n=125 cells
848 (remodeling plexus) from 4 independent retinas from n ≥3 mice per genotype.
849 Statistical analysis was performed by Pearson correlation coefficient.
850 (**G**) Representative images of P8 retinas isolated from control and C2β$^{KI/KI}$ mice treated
851 with rapamycin on P6 and P7. Vehicle was injected into littermates. Retinas were

852 immunostained for p-S6-Ser$^{235/236}$ (white) and blood vessels were marked with IB4
853 (red). Scale bars: 150 μm (upper panel), 30 μm (middle and lower panels).
854 (**H,I**) Quantification of p-S6-Ser$^{235/236}$ intensity in blood vessels (**H**) and vascular
855 density by IB4-positive area (**I**). n ≥ 5 retinas from n ≥3 mice per genotype.
856 All error bars are s.e.m. Statistical analysis was performed by two-tailed Mann-
857 Whitney test. *p ≤ 0.05, **p ≤ 0.01 and ***p ≤ 0.001.
858
859 **Figure 6. The role of PI3K-C2β in endothelial cells during retinal sprouting**
860 **angiogenesis.**
861 Endothelial cell growth during angiogenesis is tightly regulated by the PI3K-
862 2Cβ/mTORC1 axis. Lysosome-bound PI3K-C2β-generated phospholipid, PI(3,4)P_2,
863 recruits 14-3-3 that couples with mTORC1 complex through Raptor. This interaction
864 fine-tunes the cellular outcome of mTORC1-induced signaling, restricting cell growth.
865 In contrast, loss of PI3K-C2β activity accelerates mTORC1 signaling by limiting the
866 interaction with 14-3-3 protein, resulting in increased endothelial cell growth and
867 consequently retina vascularity.

Figure 1

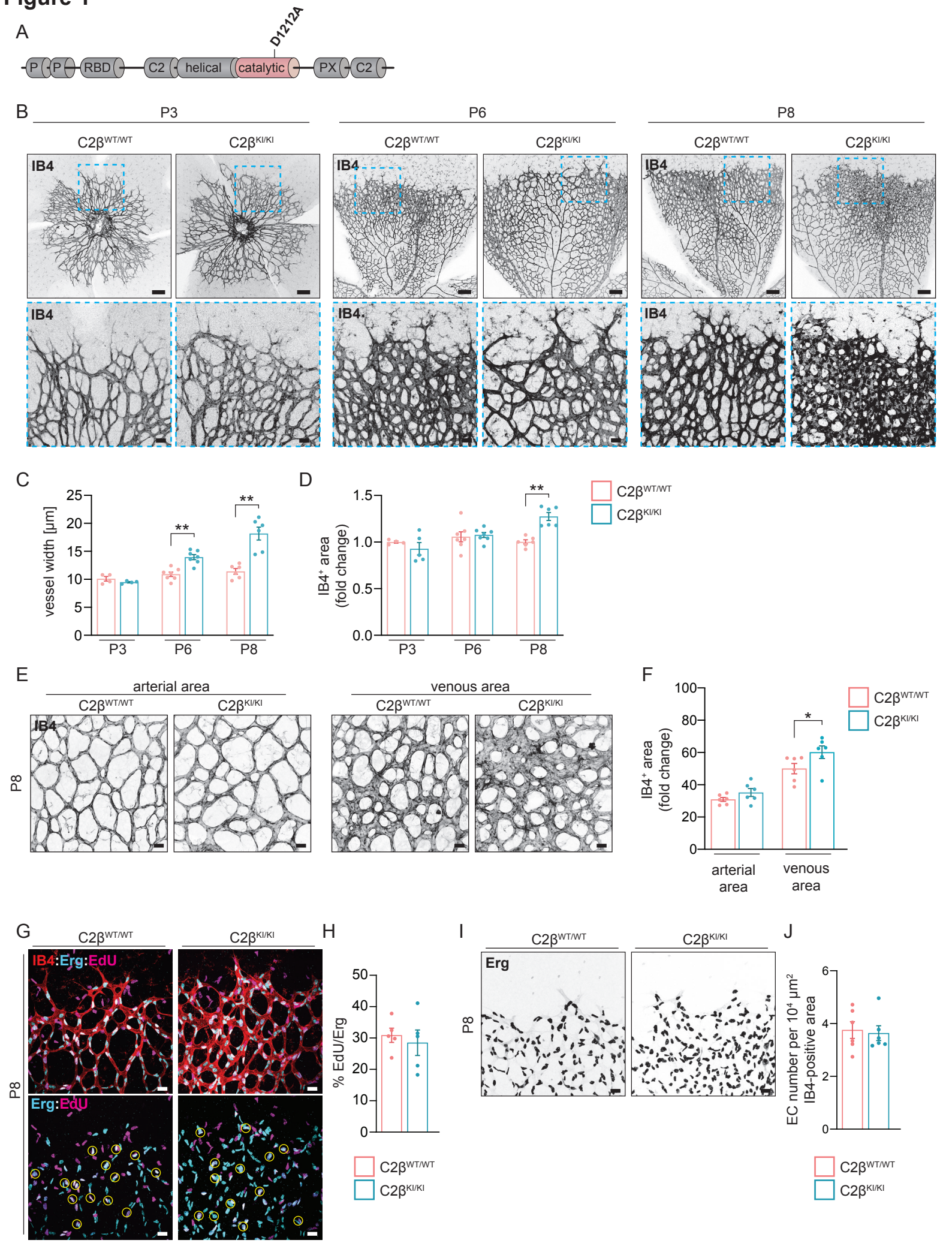
A
D1212A
P
P
RBD
C2
helical
catalytic
PX
C2
B
P3
P6
P8
C2β^WT/WT
C2β^KI/KI
IB4
C
vessel width [μm]
25
20
15
10
5
0
**
**
P3
P6
P8
D
IB4⁺ area (fold change)
1.5
1.0
0.5
0.0
**
P3
P6
P8
C2β^WT/WT
C2β^KI/KI
E
arterial area
venous area
C2β^WT/WT
C2β^KI/KI
IB4
P8
F
IB4⁺ area (fold change)
100
80
60
40
20
0
*
arterial area
venous area
C2β^WT/WT
C2β^KI/KI
G
C2β^WT/WT
C2β^KI/KI
IB4:Erg:EdU
Erg:EdU
P8
H
% EdU/Erg
50
40
30
20
10
0
C2β^WT/WT
C2β^KI/KI
I
C2β^WT/WT
C2β^KI/KI
Erg
P8
J
EC number per 10⁴ μm² IB4-positive area
6
4
2
0
C2β^WT/WT
C2β^KI/KI

Figure 2

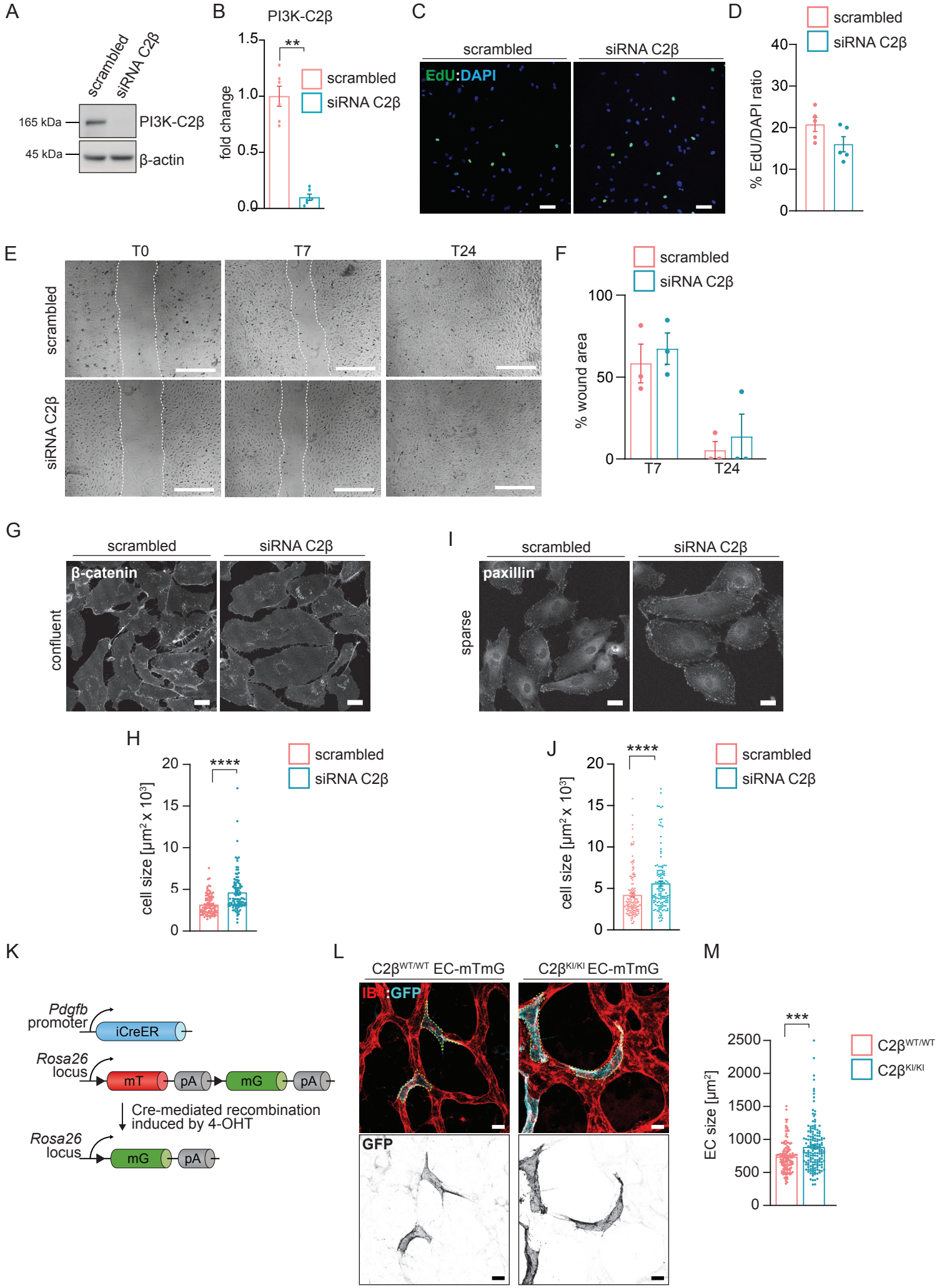
A
scrambled
siRNA C2β
165 kDa
PI3K-C2β
45 kDa
β-actin
B
PI3K-C2β
fold change
1.5
1.0
0.5
0.0
**
scrambled
siRNA C2β
C
scrambled
siRNA C2β
EdU:DAPI
D
scrambled
siRNA C2β
% EdU/DAPI ratio
40
30
20
10
0
E
T0
T7
T24
scrambled
siRNA C2β
F
scrambled
siRNA C2β
% wound area
100
50
0
T7
T24
G
scrambled
siRNA C2β
β-catenin
confluent
I
scrambled
siRNA C2β
paxillin
sparse
H
cell size [μm² x 10³]
20
15
10
5
0
****
scrambled
siRNA C2β
J
cell size [μm² x 10³]
20
15
10
5
0
****
scrambled
siRNA C2β
K
Pdgfb
promoter
iCreER
Rosa26
locus
mT
pA
mG
pA
Cre-mediated recombination
induced by 4-OHT
Rosa26
locus
mG
pA
L
C2β^WT/WT EC-mTmG
C2β^KI/KI EC-mTmG
IB4:GFP
GFP
M
EC size [μm²]
2500
2000
1500
1000
500
0
***
C2β^WT/WT
C2β^KI/KI

Figure 3

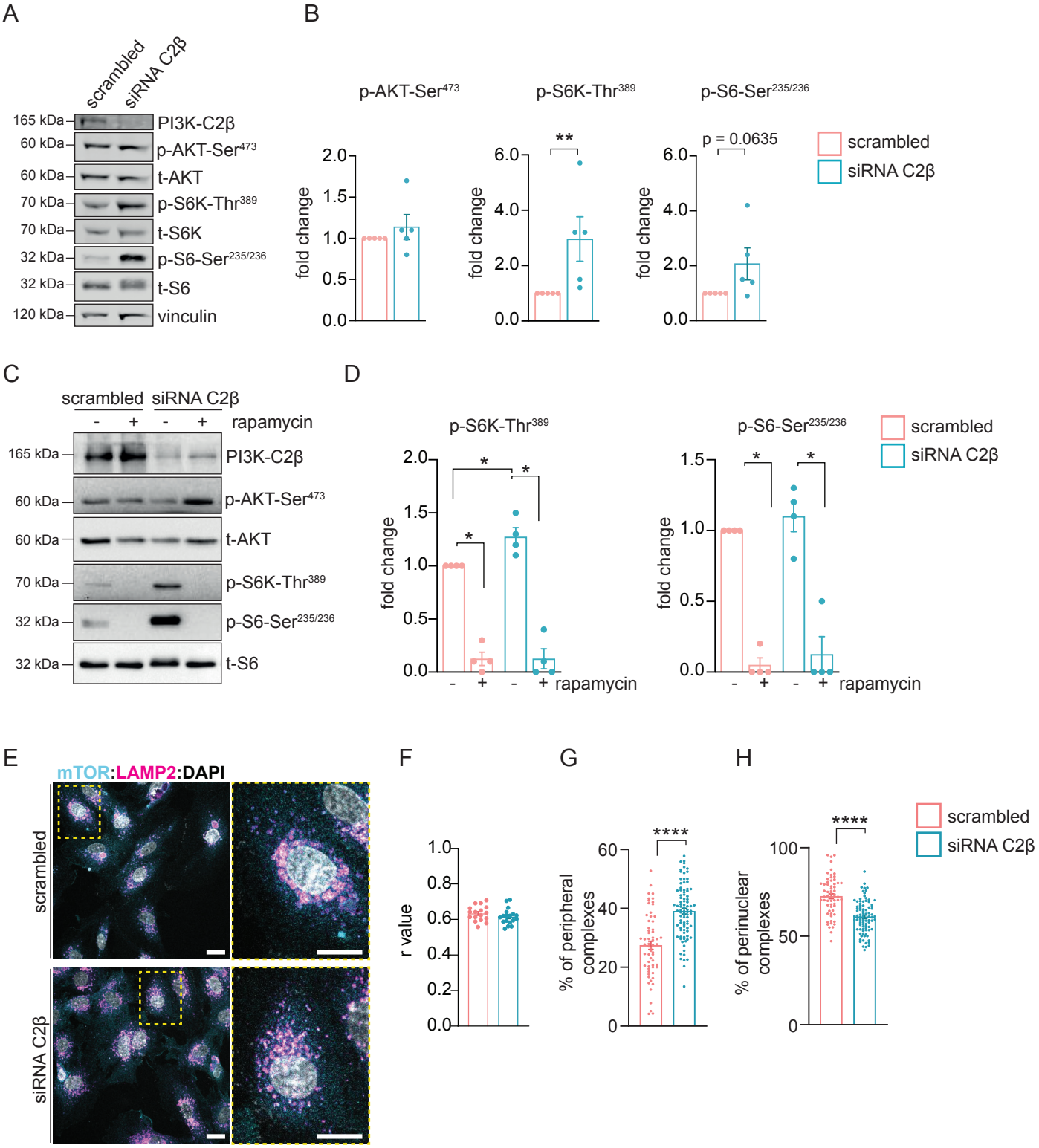
A
scrambled
siRNA C2β
165 kDa
PI3K-C2β
60 kDa
p-AKT-Ser473
60 kDa
t-AKT
70 kDa
p-S6K-Thr389
70 kDa
t-S6K
32 kDa
p-S6-Ser235/236
32 kDa
t-S6
120 kDa
vinculin
B
p-AKT-Ser473
p-S6K-Thr389
p-S6-Ser235/236
fold change
**
p = 0.0635
scrambled
siRNA C2β
C
scrambled
siRNA C2β
rapamycin
PI3K-C2β
p-AKT-Ser473
t-AKT
p-S6K-Thr389
p-S6-Ser235/236
t-S6
D
p-S6K-Thr389
p-S6-Ser235/236
fold change
rapamycin
E
mTOR:LAMP2:DAPI
scrambled
siRNA C2β
F
r value
G
% of peripheral complexes
****
H
% of perinuclear complexes
****
scrambled
siRNA C2β

Figure 4

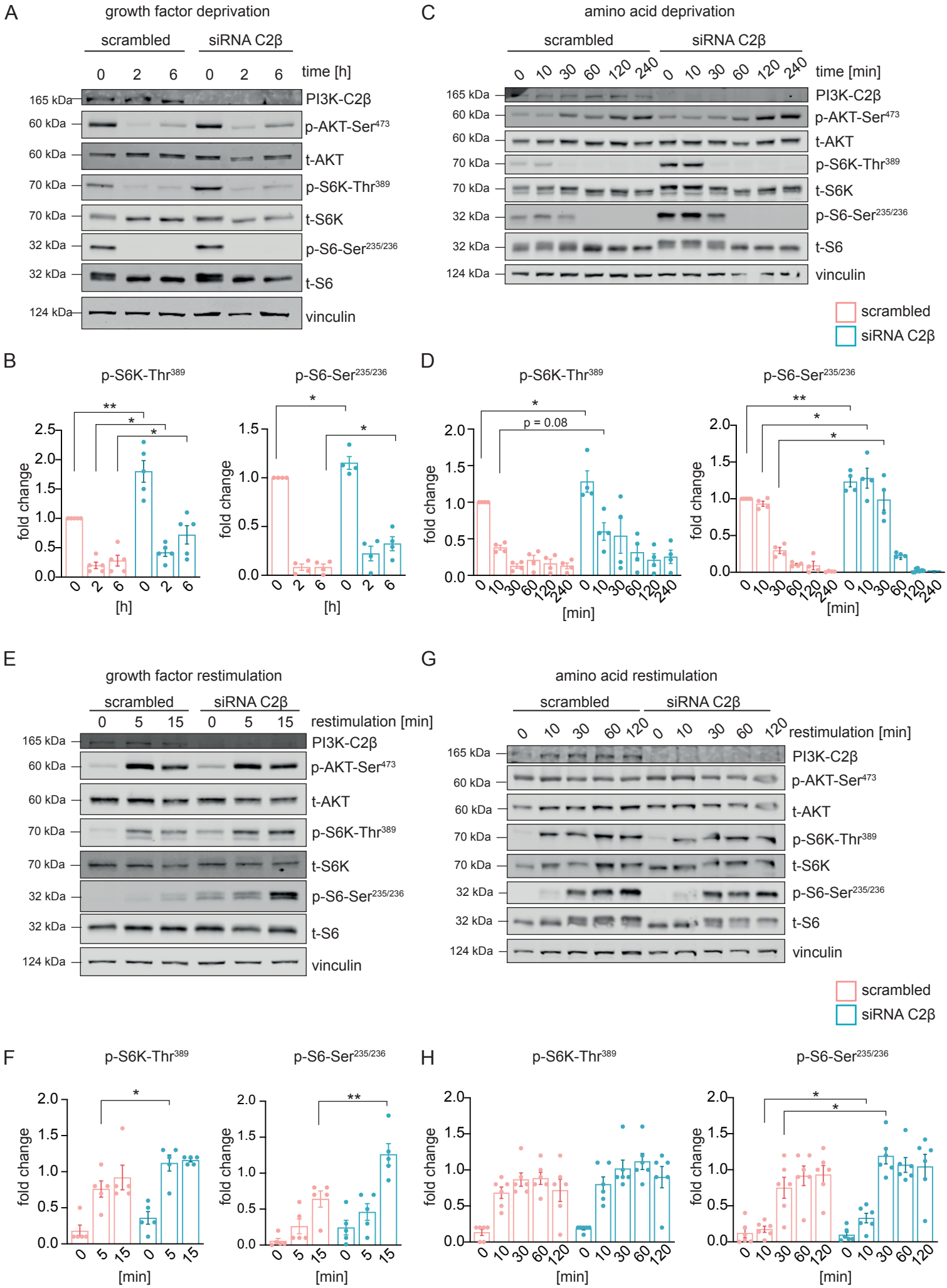
A
growth factor deprivation
scrambled
siRNA C2β
0 2 6 0 2 6
time [h]
165 kDa PI3K-C2β
60 kDa p-AKT-Ser473
60 kDa t-AKT
70 kDa p-S6K-Thr389
70 kDa t-S6K
32 kDa p-S6-Ser235/236
32 kDa t-S6
124 kDa vinculin
B
p-S6K-Thr389
p-S6-Ser235/236
fold change
[h]
C
amino acid deprivation
scrambled
siRNA C2β
0 10 30 60 120 240 0 10 30 60 120 240
time [min]
165 kDa PI3K-C2β
60 kDa p-AKT-Ser473
60 kDa t-AKT
70 kDa p-S6K-Thr389
70 kDa t-S6K
32 kDa p-S6-Ser235/236
32 kDa t-S6
124 kDa vinculin
scrambled
siRNA C2β
D
p-S6K-Thr389
p-S6-Ser235/236
p = 0.08
fold change
[min]
E
growth factor restimulation
scrambled
siRNA C2β
0 5 15 0 5 15
restimulation [min]
165 kDa PI3K-C2β
60 kDa p-AKT-Ser473
60 kDa t-AKT
70 kDa p-S6K-Thr389
70 kDa t-S6K
32 kDa p-S6-Ser235/236
32 kDa t-S6
124 kDa vinculin
G
amino acid restimulation
scrambled
siRNA C2β
0 10 30 60 120 0 10 30 60 120
restimulation [min]
165 kDa PI3K-C2β
60 kDa p-AKT-Ser473
60 kDa t-AKT
70 kDa p-S6K-Thr389
70 kDa t-S6K
32 kDa p-S6-Ser235/236
32 kDa t-S6
124 kDa vinculin
scrambled
siRNA C2β
F
p-S6K-Thr389
p-S6-Ser235/236
fold change
[min]
H
p-S6K-Thr389
p-S6-Ser235/236
fold change
[min]

Figure 5

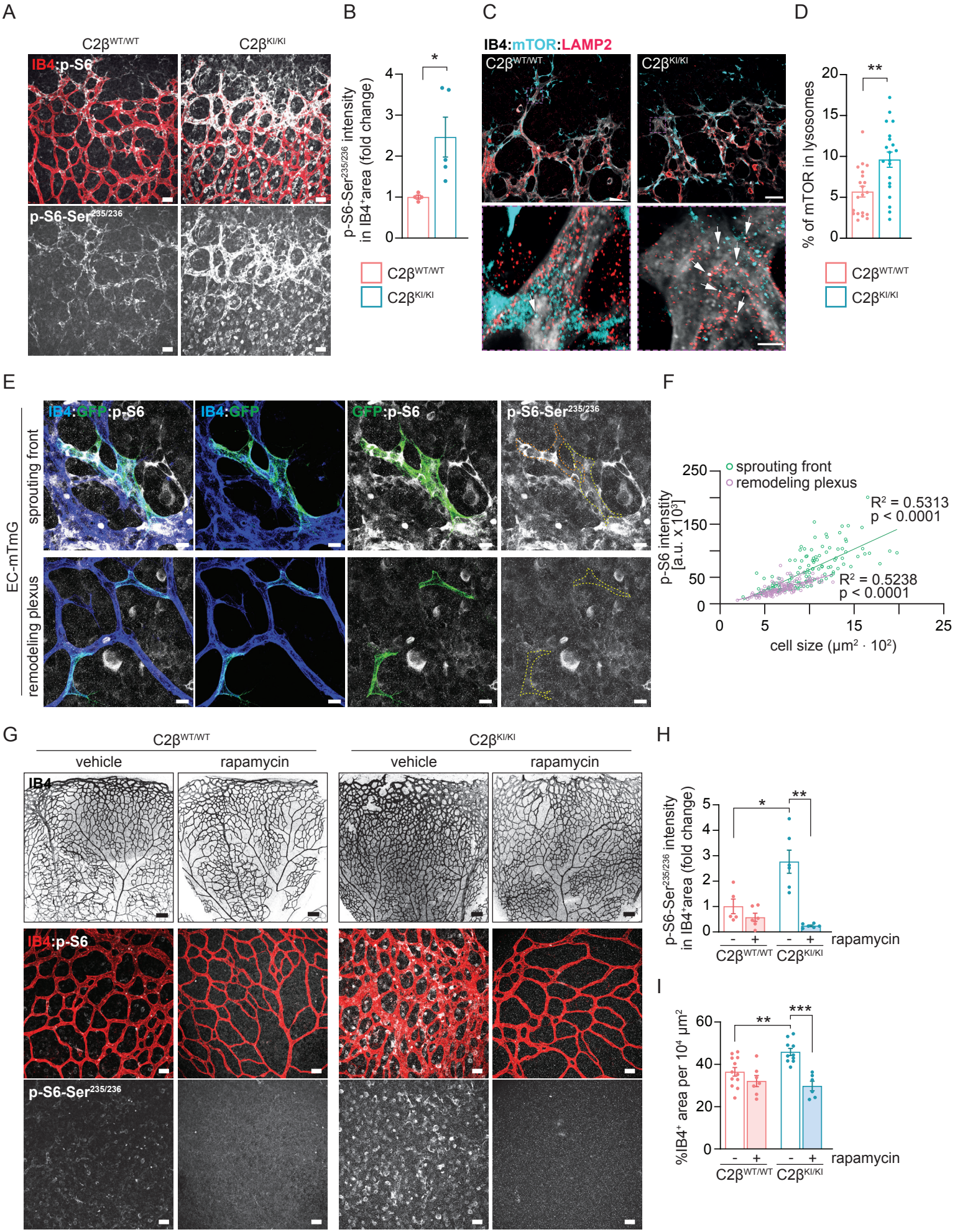
A
C2β^WT/WT
C2β^KI/KI
IB4:p-S6
p-S6-Ser^235/236
B
p-S6-Ser^235/236 intensity in IB4+area (fold change)
*
C2β^WT/WT
C2β^KI/KI
C
IB4:mTOR:LAMP2
C2β^WT/WT
C2β^KI/KI
D
% of mTOR in lysosomes
**
C2β^WT/WT
C2β^KI/KI
E
EC-mTmG
sprouting front
remodeling plexus
IB4:GFP:p-S6
IB4:GFP
GFP:p-S6
p-S6-Ser^235/236
F
sprouting front
remodeling plexus
R² = 0.5313
p < 0.0001
R² = 0.5238
p < 0.0001
p-S6 intensity [a.u. x 10³]
cell size (μm² · 10²)
G
C2β^WT/WT
C2β^KI/KI
vehicle
rapamycin
IB4
IB4:p-S6
p-S6-Ser^235/236
H
p-S6-Ser^235/236 intensity in IB4+area (fold change)
*
**
rapamycin
C2β^WT/WT
C2β^KI/KI
I
%IB4+ area per 10⁴ μm²
**
***
rapamycin
C2β^WT/WT
C2β^KI/KI

Figure 6

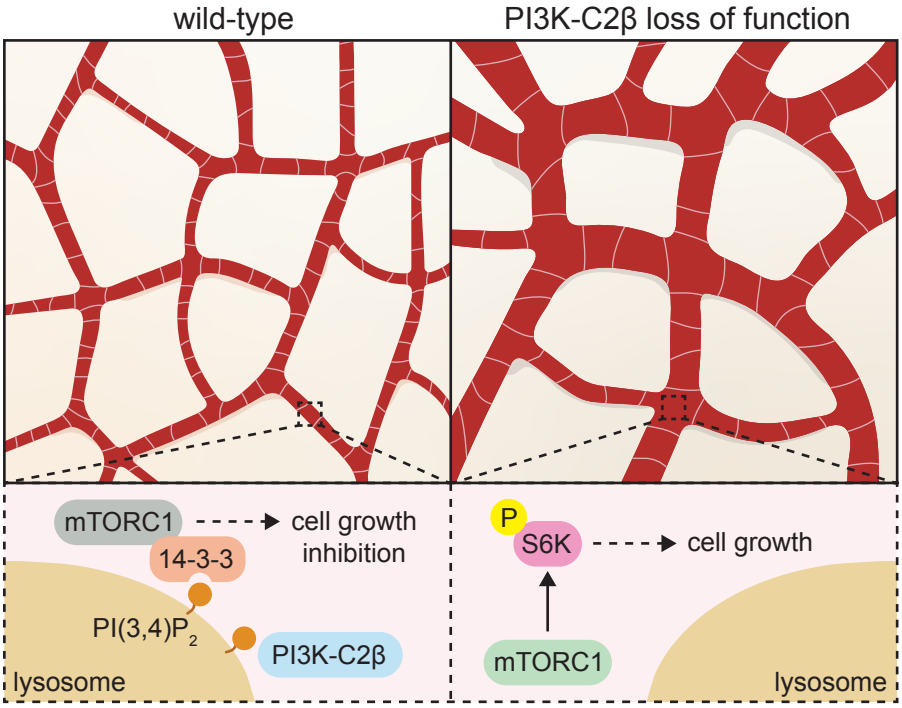
wild-type
PI3K-C2β loss of function
mTORC1
cell growth inhibition
14-3-3
PI(3,4)P2
PI3K-C2β
lysosome
P
S6K
cell growth
mTORC1
lysosome